doi: 10.3969/j.issn.0490-6756.2017.03.030

g-C_3N_4-P25 有机-无机复合物制备及可见光诱导光催化转化 CO_2 性能研究

万丽娟[1,2], 杨　明[3]
(1. 南京交通职业技术学院, 南京 211188; 2. 江苏省交通节能减排工程技术研究中心, 南京 211188;
3. 东南大学交通学院, 南京 210096)

摘　要: 通过简单混合和热处理方法合成了不同 g-C_3N_4 含量的 g-C_3N_4-P25 有机—无机复合物。通过 XRD、HRTEM、紫外-可见漫反射光谱、红外光谱、XPS 光谱和比表面测试对复合光催化剂进行表征。测试结果表明在可见光照射下,含 60%或 80% g-C_3N_4 的 g-C_3N_4-P25 复合光催化剂的光催化还原 CO_2 的活性高于单相的 g-C_3N_4 或 P25。合成的有机—无机复合物具有高的光催化活性是由于提高了半导体界面和内部电子-空穴对的分离。

关键词: 光催化; g-C_3N_4; 复合物
中图分类号: O643.3　　**文献标识码**: A　　**文章编号**: 0490-6756(2017)03-0605-06

g-C_3N_4 and P25 organic-inorganic composite for improved visible light-induced photocatalytic conversion of CO_2

WAN Li-Juan[1,2], *YANG Ming*[3]
(1. Nanjing Vocational Institute of Transport Technology, Nanjing 211188, China; 2. Jiangsu Engineering Technology Research Center for Energy Conservation and Emission Reduction of Transportation, Nanjing 211188, China;
3. School of Transportation, Southeast University, Nanjing 210096, China)

Abstract: g-C_3N_4 and P25 organic-inorganic composite with varying the content of g-C_3N_4 has been synthesized through facile mixing and heating method. The composite was characterized by X-ray diffraction, high-resolution transmission electron microscopy (HRTEM) and UV-vis diffuse reflection spectroscopy, Fourier transform infrared (FT-IR) spectroscopy, X-ray photoelectron spectroscopy (XPS) and BET surface area measurements. The activity of composite photocatalyst g-C_3N_4-P25 with 60% or 80% g-C_3N_4 for photoreduction of CO_2 is higher than that of either single-phase g-C_3N_4 or P25 under visible light irradiation. The as-prepared organic-inorganic composite exhibits an improved photocatalytic activity due to enhancement of electron-hole separations both at the interface and in the semiconductors.
Keywords: Photocatalysis; g-C_3N_4; Composite

1　Introduction

In recent years, the photocatalysis technique has a promising application for the removal of contamination, water splitting for hydrogen generation, and also photoreduction of CO_2 into fuels

收稿日期: 2016-04-13
基金项目: 江苏省高等学校自然科学研究项目(16KJD610004), 国家自然科学基金(5120812),南京交通职业技术学院高层次人才科研启动人才科研启动经费项目
作者简介: 万丽娟(1978－), 女, 山东章丘人, 助理研究员, 博士, 研究方向为环境科学. E-mail:bartty_ym@163.com

by using solar energy. The photogenerated electron-hole pairs form and transfer to the surface of semiconductor under light irradiation, which gives rise to the photooxidation-reduction reaction[1]. While, the key factor to realize the technique for large-scale industrial application is to obtain highly efficient and low-cost photocatalysts. So far, various techniques, such as increasing surface area[2,3], element doping[4-6], loading cocatalyst[7,8] and forming solid solution[9-11], were used to improve the photocatalytic activity for the photocatalyst.

Recently, an organic polymer photocatalyst, graphite-like carbon nitride ($g\text{-}C_3N_4$), has been reported[12], which possesses the performance of hydrogen or oxygen production from water splitting and the removal of pollutants[13,14] under visible light irradiation, and such low-cost photocatalysis materials have potential application in the field of civil engineering. The simple polymer catalyst may have potential applications in photocatalysis field if some methods can be found for improving the photocatalytic activity of this catalyst. Some composite catalysts have shown better catalytic activity than that of single component catalyst, e.g., $g\text{-}C_3N_4$ and TaON composite photocatalyst was prepared and showed better photocatalytic activity for photodegradation of rhodamine B than $g\text{-}C_3N_4$ or TaON[15]; Other composite photocatalysts such as graphene/C_3N_4[16,17], $g\text{-}C_3N_4/Bi_2WO_6$[18], $g\text{-}C_3N_4\text{-}SrTiO_3:Rh$[19], MWNTs/$g\text{-}C_3N_4$[20], $g\text{-}C_3N_4/ZnO$[21], $BiOBr\text{-}C_3N_4$[22], $g\text{-}C_3N_4/SmVO_4$[23] and AgX/$g\text{-}C_3N_4$ (X = Br, I)[24] have been synthesized. $g\text{-}C_3N_4$ and TiO_2 composite showed better performance for photocatalytic H_2 evolution under visible light irradiation than $g\text{-}C_3N_4$ or TiO_2[25]. Furthermore, in situ synthesis of graphitic carbon nitride ($g\text{-}C_3N_4$)-N-TiO_2 heterojunction as an efficient photocatalyst for photoreduction of CO_2 has been reported[26]. Therefore, it is expected to further improve the photocatalytic activity of $g\text{-}C_3N_4$ through forming composite photocatalysts. Using simple mixing-heating method to prepare the $g\text{-}C_3N_4$ and P25 composite and studying the photoreduction of CO_2 has not been reported till now. In this paper, $g\text{-}C_3N_4$ and P25 composite photocatalysts with varying the content of $g\text{-}C_3N_4$ were prepared. Based on the experimental results, the possible mechanism for the improved photocatalytic activity in photoreduction reactions of CO_2 was proposed.

2 Experimental

Synthesis of $g\text{-}C_3N_4$-P25 composite: In a typical process, the photocatalyst of $g\text{-}C_3N_4$ was prepared by directly heating melamine at 500 °C (heating rate: 20 °C /min) for 2 h, and the further deammonation treatment was set at 520 °C for 2 h[13], respectively in the semiclosed system to prevent sublimation of melamine. The P25 (TiO_2, commercial degussa P25) and $g\text{-}C_3N_4$ powders were mixed by ball-milling and then calcined at 400 °C for 2 h in a muffle furnace.

Characterization of samples: The products were characterized by X-ray diffraction (XRD) for phase identification on a Rigaku Ultima III diffractometer with Cu $K\alpha$ radiation (λ = 0.154 nm, 40 kV, 40 mA) and a scan rate of 10 °·min^{-1}. X-ray photoelectron spectroscopy (XPS) data were collected on a THERMO FISHER SCIENTIFIC K-Alpha instrument. The specific surface area of the as-prepared powders was obtained on a Micromeritics TriStar 3000 instrument (USA) at 77 K and Brunauer-Emmett-Teller (BET) equation was used to calculate the specific surface area. The infrared optical properties were measured on NEXUS870 IR spectrometer using KBr pellet technique. Ultraviolet visible (UV-vis) diffuse reflection spectra were measured using a UV-vis spectrophotometer (Shimadzu UV-2550, Japan) and converted from reflection to absorbance by the Kubelka-Munk method. The microstructure of the sample was observed by a high resolution transmission electron microscope (HR-TEM; JEM-2100, 200 kV, JEOL Ltd.).

In the photocatalytic reduction of CO_2, the composite powder (0.1 g) was uniformly dispersed on a glass reactor with an area of 4.2 cm^2. The

light irradiation system contains a 300 W Xe lamp with cut-off filter L42 for visible light. The volume of the reaction system was about 230 mL. The reaction setup was vacuum-treated for several times, and then high-purity CO_2 gas was introduced into the reaction to achieve ambient pressure. Deionized water (0.4 mL) was injected into the reaction system as reducing agent. About 1 mL of gas during the irradiation was taken from the reaction cell at given intervals for subsequent CO concentration analysis with a gas chromatograph (GC-2014, Shimadzu Corp., Japan).

3 Results and discussion

The powder XRD patterns of g-C_3N_4, P25 and g-C_3N_4-P25 composites are shown in Fig. 1. It can be seen that there are two peaks in sample with 100% g-C_3N_4 at 27.41° and 13.08°, which can be indexed to (002) peak (the characteristic inter-layer staking peak of aromatic systems) and (100) diffraction planes (the in-plane structural packing motif) of the graphite-like carbon nitride[13] respectively. No impurity phase was observed in the pure P25 sample, which is consistent with the XRD pattern of anatase (JCPDS No. 21-1272) and rutile (JCPDS No. 21-1276) mixed phases. The g-C_3N_4-P25 composite samples present a two composition: g-C_3N_4 and P25, and with the increase of the content of g-C_3N_4, the intensity of the (002) peak becomes stronger.

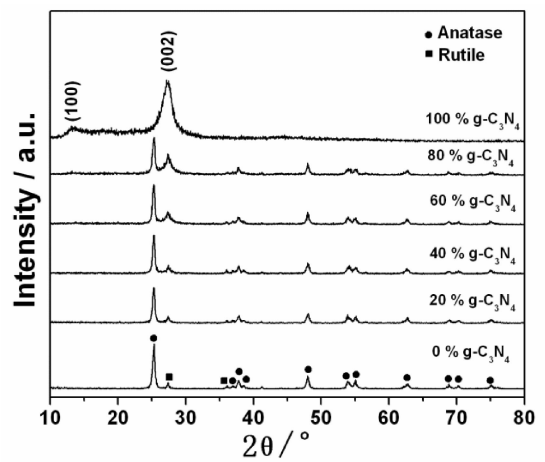

Fig. 1　XRD patterns of the P25 and g-C_3N_4 composites with different proportions

Fig. 2 shows the Fourier transform infrared (FT-IR) spectra of g-C_3N_4, P25 and g-C_3N_4-P25 composites respectively. The FT-IR spectra of the as-prepared g-C_3N_4 show the features very similar to those of the published results[25]. The absorption band near 1640 cm^{-1} is attributed to C-N stretching, while other three absorption bands near 1240, 1320 and 1408 cm^{-1} are attributed to aromatic C-N stretching. A broad band near 3140 cm^{-1} corresponds to the stretching modes of terminal NH_2 or NH groups at the defect sites of the aromatic ring[25]. The band near 810 cm^{-1} is attributed to out-of plane modes of C-N heterocycles. The FT-IR spectra of g-C_3N_4-P25 composites show that the intensities of the peaks at 810, 1240, 1320, 1408 and 1640 cm^{-1} which are attributed to g-C_3N_4 become stronger with the increase of the content of g-C_3N_4. And for the pure P25, the broad absorption band near 500-1000 cm^{-1} is clearly shown, which is attributed to the stretching vibration of Ti-O-Ti bond[27].

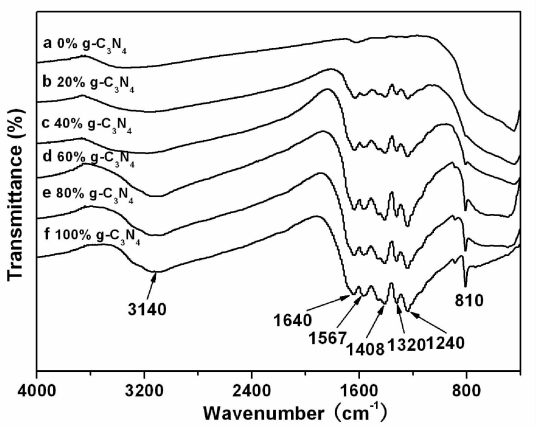

Fig. 2　FTIR spectra of the P25 and g-C_3N_4 composites with different proportions

UV-vis diffuse reflectance spectroscopy was used to investigate the optical properties of the samples. Fig. 3 shows the UV-vis absorption spectra of g-C_3N_4, P25 and g-C_3N_4-P25 composites. The absorption edge of the P25 sample occurs at ca. 380 nm, and the band gap energy is estimated to be 3.26 eV. After coupled with g-C_3N_4, the absorption edge shifts to the lower energy region. It can be seen that the absorption edges of the composite samples shift remarkably to longer wavelength with increasing the

amount of g-C_3N_4. The decrease in band gaps of the samples is from 3.26 eV of P25 to 2.70 eV of g-C_3N_4 when the content of g-C_3N_4 is increased from 0% to 100%.

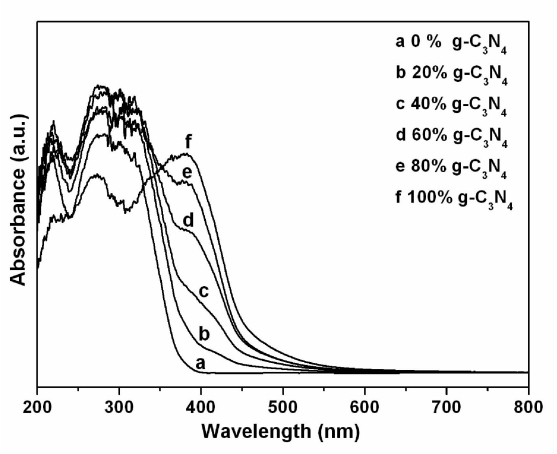

Fig. 3 The UV-vis diffuse reflectance spectra of the P25 and g-C_3N_4 composites with different proportions

The morphology of 60 wt.% g-C_3N_4-P25 composite material was investigated using TEM and high-resolution TEM (HRTEM), as shown in Fig. 4a and b respectively. The particle size of the P25 was estimated to be in the range of approximately 20-40 nm. The HRTEM image (Fig. 4b) shows that the lattice fringes have a spacing of 0.352 nm corresponding to interplanar spacing of (101) plane of anatase TiO_2.

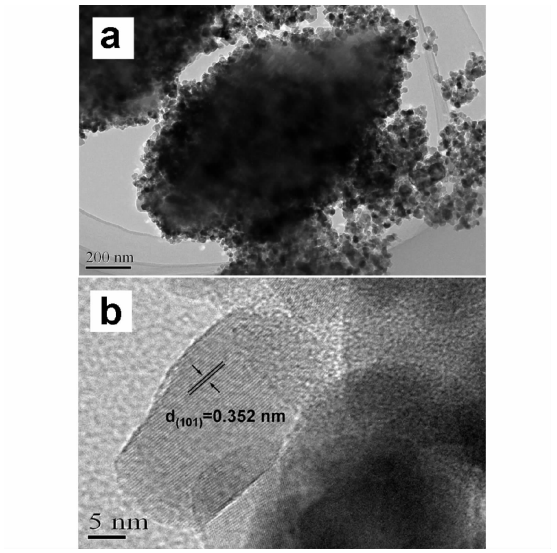

Fig. 4 TEM image (a) and the high-resolution TEM image (b) of the 60 wt.% g-C_3N_4-P25 composite

Fig. 5 shows that CO_2 can be photoreduced to CO in the presence of water vapor by using the above-mentioned g-C_3N_4-P25 composite samples as photocatalysts. From Fig. 5, it is obvious that 60 wt.% g-C_3N_4-P25 (301.4 ppm h^{-1} CO) and 80 wt.% g-C_3N_4-P25 (166.2 ppm h^{-1} CO) exhibit higher activity than g-C_3N_4 (106.4 ppm h^{-1} CO). The mechanism of photoreduction of CO_2 into CO can be described as follows: under the visible light irradiation, the photogenerated hole on the valence band top (potential: 1.50 V vs. NHE got from the XPS VB spectrum shown in Fig. 6) of g-C_3N_4 can lead to the oxidation of water to produce hydrogen ions via $H_2O \rightarrow 1/2O_2 + 2H^+ + 2e^-$ ($E^{\circ}_{redox} = 0.82$ V vs. NHE)[28], and the photogenerated electron on the conduction band bottom (potential: −1.20 V vs. NHE) of g-C_3N_4 can drive the reduction of CO_2 into CO via $CO_2 + 2e^- + 2H^+ \rightarrow CO + H_2O$ ($E^{\circ}_{redox} = -0.53$ V vs. NHE)[28]. The BET specific surface area of the g-C_3N_4, 20, 40, 60 and 80 wt.% g-C_3N_4-P25 samples is 8.2, 44.4, 37.3, 28.2, 21.6 $m^2 \cdot g^{-1}$, respectively. Thus, the improved photocatalytic activity is not attributed to the effect of the specific surface areas. The enhancement of performance of the composite materials is supposed to be attributed to the more effective separation of the photogenerated electron-hole pairs. From Fig. 5, the photocatalytic activity of 60 wt.% g-C_3N_4-P25 sample is much higher than that of 80 wt.% g-C_3N_4-P25 composite. For the g-C_3N_4-P25 composite, the content of g-C_3N_4 was important to achieve the high photocatalytic activity. The suitable content of g-C_3N_4 caused the better dispersion of P25, and that may promote the transfer and separation of photogenerated electrons and holes. However, at content higher than 60 wt.%, the heterojunction structures and interfaces between g-C_3N_4 and P25 particles decreased and thus the interfacial charge transfer was suppressed, which reduced the photocatalytic activity.

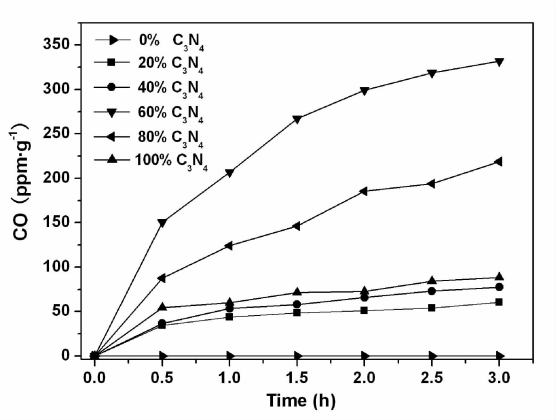

Fig. 5　CO_2 photoreduction over the P25 and g-C_3N_4 composites with different proportions

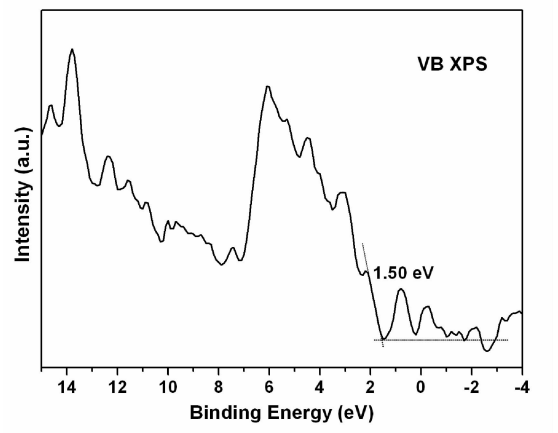

Fig. 6　VB XPS spectrum of g-C_3N_4

The scheme for electron-hole separation and transport at the g-C_3N_4-P25 composite photocatalyst interface is shown in Fig. 7. As shown in Fig. 7, the CB and VB edge potentials of g-C_3N_4 are at −1.20 and 1.50 eV, respectively. The CB and VB edge potentials of TiO_2 are at −0.29 and 2.91 eV, respectively[25]. Under irradiation by simulated sunlight, electrons are excited from VB to CB in both g-C_3N_4 and TiO_2, generating holes in the VBs of both semiconductors. The photogenerated electrons in g-C_3N_4 can easily migrate to the TiO_2 surface. This process can effectively improve the separation of photogenerated electron-hole pair and greatly decrease the possibility of photogenerated charge recombination, resulting in the high photoactivity of g-C_3N_4-P25 composites. This mechanism also explains the promotion effects of TiO_2 under visible light. Under the irradiation of visible light, only g-C_3N_4 can generate electron-hole pairs for photocatalytic CO_2 reduction. Since the CB edge potential of g-C_3N_4 (−1.20 eV) is more negative than that of TiO_2 (−0.29 eV), the photogenerated electrons on g-C_3N_4 particle surfaces transfer more easily to TiO_2 via the well developed interface and reduce CO_2 to CO.

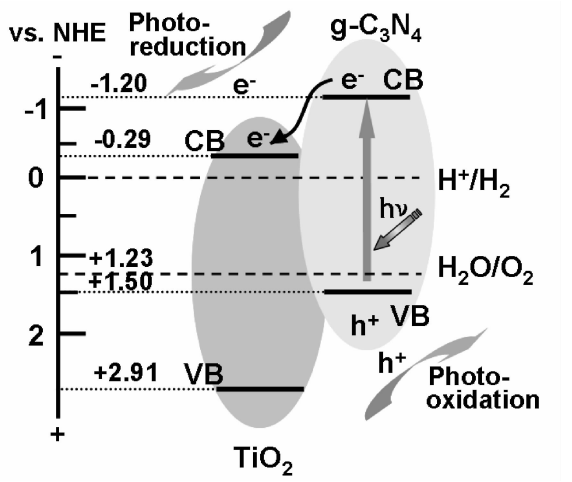

Fig. 7　The schematic illustration for the electron-hole separation and transport at the g-C_3N_4-P25 composite photocatalyst interface.

4　Conclusions

In summary, the g-C_3N_4-P25 composite materials with varying the content of g-C_3N_4 were prepared. The absorption edge of the coupling materials shifts to the lower energy region compared with pure P25 and to longer wavelengths with increasing the amount of g-C_3N_4. The photocatalytic result shows that the visible light-induced reduction of CO_2 rate is remarkably enhanced by coupling P25 with g-C_3N_4 due to the effective separation of photogenerated electron-hole pairs.

References:

[1]　Schwitzgebel J, Ekerdt J G, Gerischer H, *et al*. Role of the oxygen molecule and of the photogenerated electron in TiO_2-photocatalyzed air oxidation reactions [J]. J Phy Chem, 1995, 99(15): 5633.

[2]　Bosc F, Ayral A, Albouy P A, *et al*. A simple route for low-temperature synthesis of mesoporous and nanocrystalline anatase thin films [J]. Chem Mater, 2003, 15(12): 2463.

[3]　Antonelli D M, Ying J Y. Synthesis of hexagonally-packed mesoporous TiO_2 by a modified sol-gel method [J]. Angew Chem Int Ed, 1995, 34(18): 2014.

[4]　Zou Z G, Ye J H, Sayama K, *et al*. Direct splitting of water under visible light iradiation with an oxide

semiconductor photocatalyst [J]. Nature, 2001, 414(6864): 625.

[5] Asahi R, Morikawa T, Ohwaki T, *et al*. Visible-light photocatalysis in nitrogen-doped titanium oxides [J]. Science, 2001, 293(5528): 269.

[6] Liu L J. Photocatalytic degradation of dyestuff wastewater by nano$Yb^{3+}-Er^{3+}/TiO_2$, J Sichuan Univ (Nat Sci Ed), 2015, 52(6):1337 (in Chinese).

[7] Sato S, White J M. Photodecomposition of water over Pt/TiO_2 catalysts [J]. Chem Phys Lett, 1980, 72(1): 83.

[8] Borgarello E, Kiwi J, Pelizzetti E, *et al*. Photochemical cleavage of water by photocatalysis [J]. Nature, 1981, 289(5794): 158.

[9] Tsuji I, Kato H, Kobayashi H, *et al*. Photocatalytic H_2 evolution under visible-light irradiation over band-structure-controlled $(CuIn)_xZn_{2(1-x)}S_2$ solid solutions [J]. J Phys Chem B, 2005, 109(15): 7323.

[10] Maeda K, Teramura K, Lu D L, *et al*. Photocatalyst releasing hydrogen from water-enhancing catalytic performance holds promise for hydrogen production by water splitting in sunlight [J]. Nature, 2006, 440(7082): 295.

[11] Wang D F, Kako T, Ye J H. Efficient photocatalytic decomposition of acetaldehyde over a solid-solution perovskite $(Ag_{0.75}Sr_{0.25})(Nb_{0.75}Ti_{0.25})O_3$ under visible-light irradiation [J]. J Am Chem Soc, 2008, 130(9): 2724.

[12] Wang X C, Maeda K, Thomas A, *et al*. A metal-free polymeric photocatalyst for hydrogen production from water under visible light [J]. Nature Mater, 2009, 8(1): 76.

[13] Yan S C, Li Z S, Zou Z G. Photodegradation performance of g-C_3N_4 fabricated by directly heating melamine [J]. Langmuir, 2009, 25(17): 10397.

[14] Yang M, Feng J Q, Huang Q. Influence of mechanical milling on photocatalytic activity of g-C_3N_4 prepared by heating melamine [J]. J Wuhan Univ Technol-Mater Sci Ed, 2010, 25(6): 914.

[15] Yan S C, Lv S B, Li Z S, *et al*. Organic-inorganic composite photocatalyst of g-C_3N_4 and TaON with improved visible light photocatalytic activities [J]. Dalton Trans, 2010, 39(6):1488.

[16] Xiang Q J, Yu J G, Jaroniec M. Preparation and enhanced visible-light photo- catalytic H_2-production activity of graphene/C_3N_4 composites [J]. J Phys Chem C, 2011, 115(15): 7355.

[17] Li X H, Chen J S, Wang X C, *et al*. Metal-free activation of dioxygen by graphene/g-C_3N_4 nanocomposites: functional dyads for selective oxidation of saturated hydrocarbons [J]. J Am Chem Soc, 2011, 133(21): 8074.

[18] Ge L, Han C C, Liu J. Novel Visible light-induced g-C_3N_4/Bi_2WO_6 composite photocatalysts for efficient degradation of methyl orange [J]. Appl Catal B: Environ, 2011, 108-109: 100.

[19] Kang H W, Lim S N, Song D S, *et al*. Organic-inorganic composite of g-C_3N_4-$SrTiO_3$: Rh photocatalyst for improved H_2 evolution under visible light irradiation [J]. Inter J Hydro Energy, 2012, 37(16): 11602.

[20] Ge L, Han C C. Synthesis of MWNTs/g-C_3N_4 composite photocatalysts with efficient visible light photocatalytic hydrogen evolution activity [J]. Appl Catal B: Environ, 2012, 117-118: 268.

[21] Liu W, Wang M L, Xu C X, *et al*. Facile Synthesis of g-C_3N_4/ZnO composite with enhanced visible light photooxidation and photoreduction properties [J]. Chem Eng J, 2012, 209: 386.

[22] Fu J, Tian Y L, Chang B B, *et al*. BiOBr-carbon nitride heterojunctions: synthesis, enhanced activity and photocatalytic mechanism [J]. J Mater Chem, 2012, 22(39): 21159.

[23] Li T T, Zhao L H, He Y M, *et al*. Synthesis of g-$C_3N_4/SmVO_4$ composite photocatalyst with improved visible light photocatalytic activities in RhB degradation [J]. Appl Catal B: Environ, 2013, 129: 255.

[24] Xu H, Yan J, Xu Y G, *et al*. Novel visible-light-driven AgX/graphite-like C_3N_4 (X = Br, I) hybrid materials with synergistic photocatalytic activity [J]. Appl Catal B: Environ, 2013, 129: 182.

[25] Yan H J, Yang H X. TiO_2-g-C_3N_4 composite materials for photocatalytic H_2 evolution under visible light irradiation [J]. J Alloys Compd, 2011, 509(4): L26.

[26] Zhou S, Liu Y, Li J M, *et al*. Facile in situ synthesis of graphitic carbon nitride (g-C_3N_4)-N-TiO_2 heterojunction as an efficient photocatalyst for the selective photoreduction of CO_2 to CO [J]. Appl Catal B: Environ, 2014, 158-159: 20.

[27] Li H S, Zhang Y P, Wang S Y, *et al*. Study on nanomagnets supported TiO_2 photocatalysts prepared by a sol-gel process in reverse microemulsion combining with solvent-thermal technique [J]. J Hazard Mater, 2009, 169(1-3): 1045.

[28] Indrakanti V P, Kubicki J D, Schobert H H. Photoinduced activation of CO_2 on Ti-based heterogeneous catalysts: current state, chemical physics-based insights and outlook [J]. Energy Environ Sci, 2009, 2(7): 745.